Fabrication and Measurements of Inductive Devices for Scanning Microwave Microscopy

T. Le Quang, D. Vasyukov, J. Hoffmann, A. Buchter, M. Zeier

Abstract— This article presents our results in fabrication and measurement of inductive devices for scanning microwave microscopy (SMM). Devices with resistance and inductance varying between 9 Ω-220 Ω and up to 200 pH were produced on SiN membrane using using clean room processes. Then, by combining actual SMM measurements performed for these devices and their simulation, we were able to test a calibration method which employs three known standards.

I. INTRODUCTION

Scanning microwave microscopy (SMM) is still a rather new member of the family of scanning probe techniques, but it has been applied successfully to the analysis of a wide range of materials [1]–[6]. The basic working principle is to send a microwave signal to the SMM tip and to measure the reflected fraction. The measured reflection coefficient, S_{11}, which is a complex number, depends on the material parameters at the tip-sample contact. Therefore, the SMM can discriminate regions with different electrical properties by showing contrast in S_{11}. Because signal reflections do not only take place at the tip-sample interface, but also at other unwanted locations, the SMM needs to be calibrated to quantify these spurious reflections prior to the conversion of S_{11} into material properties.

Among the few existing SMM calibration techniques proposed by differrent groups [7]–[9], the advantage of the one proposed in [9] is its ability to differentiate lossy and capacitive mechanisms. Modifying the idea from the short-open-load (SOL) approach used to calibrate one-port vector network analyzers (VNA), the signal loss along the SMM tip and electrical connections is modelled as a linear network with three error coefficients. We will call this calibration method mSOL. Then, values of these error coefficients can be calculated using S_{11} obtained for three samples with known impedance and the extraction of impedance of unknown devices can be performed. Later, the mSOL technique has been employed successfully in SMM measurements for n-doped GaAs samples [6].

While the mSOL method up to now has been used only for measurements on capacitive structures, we demonstrate in this article its application to characterize inductive devices, which were fabricated on a SiN membrane via the use of clean-room techniques. By tuning their shapes, we realized various values of resistance and inductance as predicted from Comsol Multiphysics simulations. Combining S_{11} obtained from SMM measurements performed on these devices and data acquired from our simulations, we were able to verify the applicability of the mSOL algorithm.

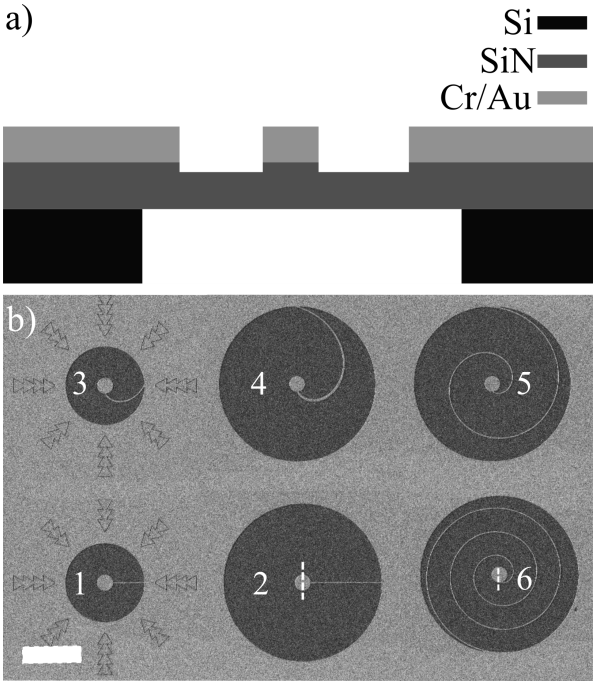

Fig. 1. a) A sketch of the cross-section view of our sample consisting of Au structures supported by a free SiN membrane. The sketch is not to scale. b) Scanning electron microscope (SEM) image of six fabricated and characterized devices, which are numbered from 1 to 6. The scale bar in (b) is 20 μm. White dashed lines are added to illustrate how we conducted our line scans to characterize devices 2 and 6. Similar measurements were also performed for other devices.

II. Sample fabrication

Fig. 1 a) presents a sketch of our sample, which consists of a 100 nm thick Cr/Au bilayer deposited on a Si substrate covered by 500 nm thick silicon nitride film. In order to suppress existing tensile stresses in deposited nitride films, a low pressure chemical vapour deposition process in a silicon-rich condition was employed to form a silicon-rich film (SiN) [10]. Metal layers were evaporated

*This project has received funding from the EMPIR programme cofinanced by the Participating States and from the European Union's Horizon 2020 research and innovation programme.

[1]T. Le Quang, D. Vasyukov, J. Hoffmann, A. Buchter, M. Zeier, RF and microwave laboratory of the Federal Institute of Metrology METAS of Switzerland, Lindenweg 50, 3003 Bern-Wabern, Switzerland. toai.lequang@metas.ch

TABLE I
Resistance and inductance calculated at 9.4 GHz for produced inductive devices

Device	Bridge	Resistance (Ω)	Inductance (pH)
1	Straight	9.08	-0.8
2	Straight	21.50	-1.1
3	Curvy	10.93	15
4	Curvy	21.79	33
5	Curvy	94.71	100
6	Curvy	221.01	208

with an e-beam evaporator and successively patterned into six different inductive devices employing ebeam lithography and dry etching with Ar ion bombardment. During the dry etching, we also slightly overetched into SiN to ensure a complete removal of the metallic film in unwanted regions. Then, by using laser lithography, we defined in the opposite side a $600\times600\,\mu m^2$ window. Then, a combination of plasma etching process and Bosch process took place to etch away Si material in this window. As reported in [6], the SMM tip can sense the inhomogeneity of dopant density of the underneath substrate. As the dopant density of our Si substrate varies between 3.3×10^{16}-$2.9\times10^{17}\,cm^{-3}$, as calculated from its resistivity (0.1-0.5 Ω·cm), the removal of Si material reduces the uncertainty of our measurements on fabricated devices. During these last etching processes, the front side was protected with a thin photoresist layer, which was afterwards stripped off using a mild and short oxygen plasma burst in the last step.

Fig. 1 b) displays a scanning electron microscope (SEM) image captured for all fabricated devices. As can be seen, each device consists of a circular island with a diameter of 4 μm connecting to a grounded external Au region by a narrow metallic bridge, which can be either straight (devices 1 and 2) or curvy (other devices). While the first two devices would have a small (almost zero) inductance, non-zero inductances are expected for other structures thanks to existing inductive couplings between various parts of their curvy brige. The introduction of additional rings does not only prolong the total length of the bridge but also leads to the increase of the inductance. Resistance and inductance of all six devices were calculated using Comsol Multiphysics and are listed in Tab. I. The negative inductances found for devices 1 and 2 are attributed to the parasitic capacitive interaction between the tip and the measured sample, which outweighs the small inductance of the straight bridge of these devices.

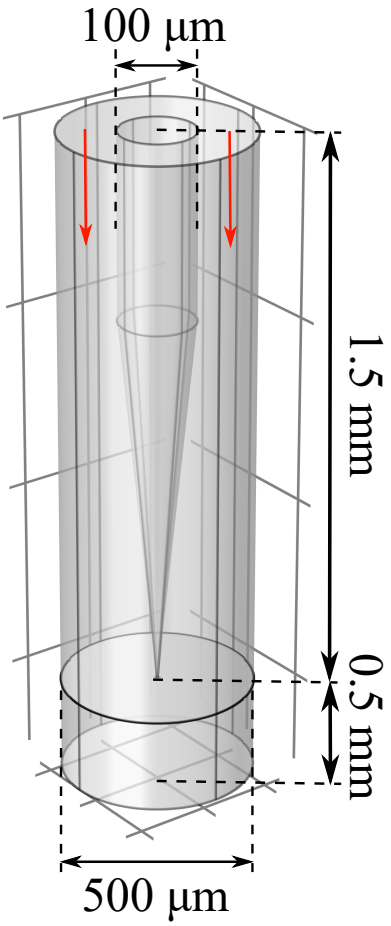

Fig. 2. A sketch of the Comsol model used to simulate our SMM measurement performed on our devices. The two red arrows are added to show how the microwave signal is injected.

III. SMM setup and Comsol Multiphysics simulations

SMM measurements were realised using a tuning fork-based setup with a few-millimeter long Platinum/Iridium (Unisoku P-100PtIr) tip with a nominal tip radius of less than 20 nm. Microwave signals with a frequency range of 1-50 GHz are generated using a Rohde & Schwarz ZVA50 VNA and are sent to the tip via coaxial cables and an impedance matching network. The whole electrical connection is less than 1 m long and is kept as fixed as possible. While measurements were performed under ambient conditions, the humidity and the temperature are controlled. More details about our setup can be found in [6].

During SMM experiments, a $1\times1\,cm^2$ sample was glued to a sample holder using silver paste. The tip was then brought close to our devices using two optical microscopes to perform measurements. While complete SMM images of each device would provide us a full spatial dependence of S_{11}, we only scanned over short lines crossing the central island of each device to avoid any potential bridge damages. For example, the characterization of devices 2 and 6 was done at 9.4 GHz by scanning along white dashed lines added in Fig. 1

b). Similar measurements were also realized for other devices.

Besides our actual SMM measurements, we also simulated these experiments using the RF module of Comsol Multiphysics. A sketch displayed in Fig. 2 is the model used in our simulations. As can be seen, in our model, the tip is in contact with the device of interest residing on a SiN disk with a diameter of 500 μm. Similar to actual measurements, the tip lands on the central island of the device and the whole system is kept in air. The outer walls of the model, except the top horizontal wall, where the microwave signal with a frequency of 9.4 GHz is injected (red arrows), are ground and are simulated using perfect electrical conductor boundary conditions. Two main simplications were employed to ensure a good and effective calculation. First, the model is restricted to only tip and sample, i.e. no cable and the tip used in our simulation is shorter (1.5 mm long), simpler (a perfect cylinder with a perfect cone-shaped head) and smaller (with a diameter of 100 μm at the contact to the VNA) than the real tip (about 1 cm long, with a rough surface and a diameter of 500 μm at the contact to the VNA). Second, we only treat one isolated device in each simulation, while real samples have many devices arranged as a two-dimensional array with a period of 50 μm.

Furthermore, using SEM images obtained for each device, we analyzed the geometry of fabricated structures with image recognition software, developed with OpenCV and Python. The analyzed results were imported into Comsol. By doing so, we were able to take into account the variation of the width of fabricated bridges. This is important, because while the straight bridge has quite a homogenous width of about 200 nm, the width of the curvy bridge varies between 200 and 300 nm, as can be seen in Fig. 1 b). Last but yet importantly, a 500 μm thick air layer below the SiN film was introduced to model the free and unsupported SiN membrane of our devices.

Besides S_{11} values provided by simulations, S_{11}^{sim}, we also calculated the impedance of our devices, which is defined as the ratio of the voltage drop on the sample surface, V, and the current, I, injected from the SMM tip into our device. V and I were calculated using following equations: $V = \int \mathbf{E}d\mathbf{l}$, and $I = \oint \mathbf{H}d\mathbf{l}$. While the line integration for V was done along a line connecting the tip and the conducting wall, we used a circle with a radius of 50 μm in a plane being 3 μm above the sample surface for the current calculation.

IV. Experimental results

Fig. 3 displays raw data (the height profile in panels a) and b) and S_{11} signals in panels c)-f)) obtained by scanning long lines crossing the central island of devices 2 and 6, respectively. These lines are white dashed lines drawn in Fig. 1 b). While we scanned along a 10 μm long line for device 2, we needed to scan over a much shorter line (5 μm) for device 6 to avoid touching and damaging our narrow bridge, which stays close to the central island. These measurements were realised at 9.4 GHz using the same tip and on the same sample under ambient condition, so that acquired data can be used to test the mSOL method.

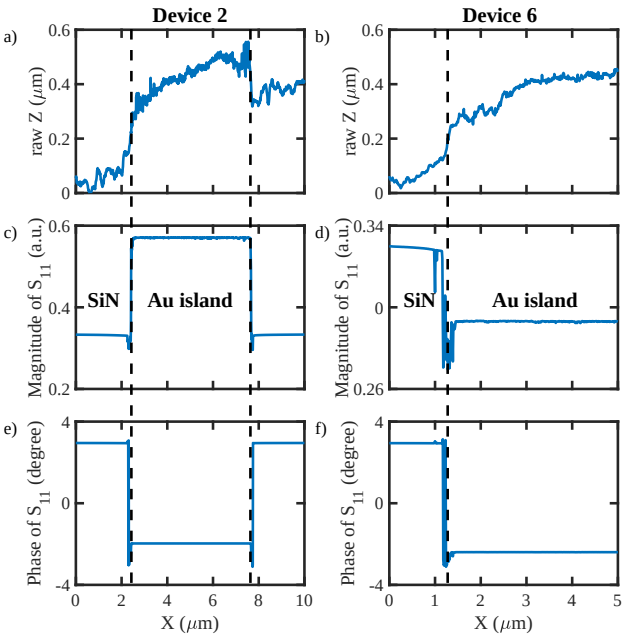

Fig. 3. a) and b)- Height profile obtained for devices 2 and 6 correspondingly. c) and d) (e) and f))- Spatial dependence of amplitude (phase) of S_{11} signals obtained for devices 2 and 6. These measurements were performed along white dashed lines shown in Fig. 1 b) with a 10 nm spatial resolution using microwave signals with a frequency of 9.4 GHz and under ambient conditions. Black dashed lines are added to mark positions of the film edge.

Positions of the film edge, marked with black dashed lines, are visible in Fig. 3 a) and b). Instead of being abrupt, edges found in both measurements extend over a 300 nm-400 nm wide region. Moreover, there is a slight difference between the value (5 μm) of the lateral size of the island measured from the profile plotted in Fig. 3 a) and the one (4 μm) obtained from SEM images in Fig. 1 b). This difference is understandable, because the height profiles plotted in Fig. 3 a) and b) are the convolution of the shape of the tip and the actual topography of the surface.

Similar conclusions about the edge region and the increase of the size of the island were drawn from S_{11} measurements both in magnitude (panels c) and d)) and in phase (panels e) and f)). A clear contrast between Au and SiN can be seen in all plotted profiles at the physical edges, as expected from the different electrical properties of these two materials.

Moreover, a comparison between S_{11} measurements acquired for devices 2 and 6 reveals different spatial dependence in the two measurements. As can be seen, Fig. 3 c) and d) displays opposite behaviours of S_{11} plots

TABLE II

S_{11}^{exp} and S_{11}^{sim} values obtained for all six devices at 9.4 GHz

Device	S_{11}^{exp} (a.u.)	S_{11}^{sim} (a.u.)
1	0.62 - 0.02i	-0.32 + 0.64i
2	0.57 - 0.02i	-0.15 + 0.44i
3	0.62 - 0.02i	-0.30 + 0.61i
4	0.55 - 0.02i	-0.14 + 0.44i
5	0.40 - 0.01i	0.34 - 0.02i
6	0.29 - 0.01i	0.60 - 0.20i

while moving from the SiN membrane into the Au film. While a strong increase (from 0.33 to 0.57) takes place at both film edges of the device 2, the magnitude of S_{11} signal drops slightly from 0.33 to 0.29 by reaching the central island of the device 6. Furthermore, the phase of S_{11} descends from 2.95° (on SiN) to -1.97° and to -2.4° for the Au island of devices 2 and 6, respectively. Same values of S_{11} acquired for SiN regions in both devices indicate that the tip is the same during these two measurements. Therefore, the difference between S_{11} signals recorded for these two inductive devices can be only attributed to their different impedance.

Similar line scans were repeated for other devices under the same conditions (tip, frequency) and same conclusions about the tip condition were drawn from the data analysis. All obtained S_{11} values were then converted into complex numbers, which are listed in Tab. II. Besides these experimental values, S_{11}^{exp}, Tab. II also includes S_{11} values produced by Comsol simulations, S_{11}^{sim}, performed for these devices. Both sets of data will be used to test the mSOL method.

V. Verification of the mSOL technique

As demonstrated in [9], the mSOL approach demands S_{11} obtained from SMM measurements performed in the same conditions for three devices with known impedance for the tip calibration. Here, we chose devices 1, 5 and 6 as standard samples to perform the calibration. Their S_{11}^{exp} (or S_{11}^{sim}) values together with their impedance (from Tab. I) were used to calibrate the SMM tip used in our actual measurement (in our simulations). Obtained error coefficients were then employed to calculate resistance and inductance of all devices from their S_{11}^{exp} (or S_{11}^{sim}), plotted as blue circles or black crosses in Fig. 4 a) and b), respectively. In the same plots, nominal values listed in Tab. I are also displayed (red dashed curves) for comparison.

As plotted in Fig. 4, data obtained using the mSOL method stay quite close to red dashed curves with certain differences. On one hand, the difference between nominal values and those obtained using the mSOL method is zero for devices 1, 5 and 6, which are used as standard samples. On the other hand, non-zero differences can be found for our unknown samples, devices 2, 3 and 4. In terms of resistance, the mSOL method reproduces well our nominal values, as the difference between blue circles (black crosses) and the red dashed line plotted in Fig. 4 a) remains low, between 1 Ω-5 Ω (and of tens of mΩ). Nevertheless, a larger deviation of about 15 pH can be found in Fig. 4 b) by comparing nominal values and data obtained with calibrated tips. Converting this value to impedance, we got an uncertainty of about 0.9 Ω, which is indeed close to the one estimated for the resistance (the real part of the impedance). Therefore, we conclude that the mSOL method is applicable for SMM measurements performed for these inductive devices.

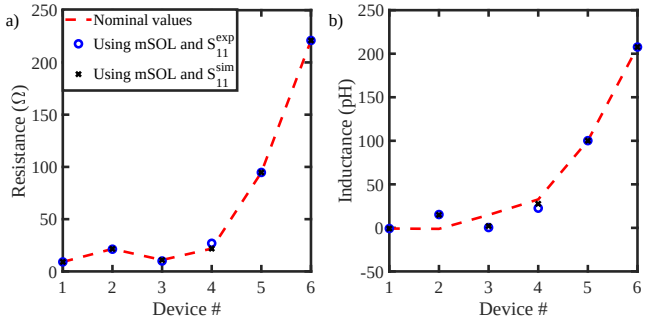

Fig. 4. Comparison between nominal values (red dashed curves) and those provided using the mSOL approach: for resistance (panel a)) and for inductance (panel b)) of fabricated devices. Blue circles and black crosses were calculated using the mSOL method together with either experimental data, S_{11}^{exp}, or values obtained from simulations, S_{11}^{sim}, respectively. Here, devices 1, 5 and 6 were used as standard samples to calibrate the SMM tips used in the actual experiments and the simulation performed with a microwave frequency of 9.4 GHz.

VI. Conclusion and Outlook

Resistive and inductive devices with a resistance between 9 Ω-220 Ω and an inductance between 0 pH-200 pH were produced on a SiN membrane. SMM characterizations were performed on these devices at 9.4 GHz and were also simulated using Comsol Multiphysics. The applicability of the mSOL calibration algorithm in SMM measurements conducted for inductive devices has been demonstrated both theoretically and experimentally. The uncertainty of less than 5 Ω and of 15 pH were obtained from our analysis. Future improvements should aim at extending further the inductance and the resistance range.

References

[1] Yalin Lu et al., Nondestructive Imaging of Dielectric-Constant Profiles and Ferroelectric Domains with a Scanning-Tip Mi-

crowave Near-Field Microscope, Science, 276, 5321, 2004-2006, 1997.
[2] M. Kasper et al., Metal-oxide-semiconductor capacitors and Schottky diodes studied with scanning microwave microscopy at 18GHz, J. Appl. Phys., 116, 184301, 2014.
[3] J. Hoffmann et al., Measuring low loss dielectric substrates with scanning probe microscopes, Appl. Phys. Lett. 105, 013102, 2014.
[4] E. Y. Ma et al., Charge-order domain walls with enhanced conductivity in a layered manganite, Nat. Commun., 6, 7595, 2015.
[5] Di Wu et al., Uncovering edge states and electrical inhomogeneity in MoS_2 field-effect transistors, PNAS, 113, 8583, 2016.
[6] A. Buchter et al., Scanning microwave microscopy applied to semiconducting GaAs structures, Rev. Sci. Instrum., 89, 023704, 2018.
[7] C. Gao and X.-D. Xiang, Quantitative microwave near-field microscopy of dielectric properties, Rev. Sci. Instrum., 69, 6, 1998.
[8] H. P. Huber et al., Calibrated nanoscale capacitance measurements using a scanning microwave microscope, Rev. Sci. Instrum., 81, 9, 2010.
[9] J. Hoffmann et al., A Calibration Algorithm for Nearfield Scanning Microwave Microscopes, IEEE-Nano, 2012.
[10] P.J French and P.M Sarro and R Mallée and E.J.M Fakkeldij and R.F Wolffenbuttel, Optimization of a low-stress silicon nitride process for surface-micromachining applications, Sensors and Actuators A: Physical, 58, 2, 149-157, 1997.